3

Thermodynamic Aspects of Precipitation Efficiency

Xinyong Shen[1] and Xiaofan Li[2]
[1]*Key Laboratory of Meteorological Disaster of Ministry of Education*
Nanjing University of Information Science and Technology
[2]*NOAA/NESDIS/Center for Satellite Applications and Research*
[1]*China*
[2]*USA*

1. Introduction

Precipitation efficiency is one of important meteorological parameters and has been widely used in operational precipitation forecasts (e.g., Doswell et al., 1996). Precipitation efficiency has been defined as the ratio of precipitation rate to the sum of all precipitation sources from water vapor budget (e.g., Auer and Marwitz, 1968; Heymsfield and Schotz, 1985; Chong and Hauser, 1989; Dowell et al., 1996; Ferrier et al., 1996; Li et al., 2002; Sui et al., 2005) after Braham (1952) calculated precipitation efficiency with the inflow of water vapor into the storm through cloud base as the rainfall source more than half century ago. Sui et al. (2007) found that the estimate of precipitation efficiency with water vapor process data can be more than 100% or negative because some rainfall sources are excluded or some rainfall sinks are included. They defined precipitation efficiency through the inclusion of all rainfall sources and the exclusion of all rainfall sinks from surface rainfall budget derived by Gao et al. (2005), which fixed precipitation efficiency to the normal range of 0-100%.

In additional to water vapor processes, thermal processes also play important roles in the development of rainfall since precipitation is determined by environmental thermodynamic conditions via cloud microphysical processes. The water vapor convergence and heat divergence and its forced vapor condensation and depositions in the precipitation systems could be major sources for precipitation while these water vapor and cloud processes could give some feedback to the environment. Gao et al. (2005) derived a water vapor related surface rainfall budget through the combination of cloud budget with water vapor budget. Gao and Li (2010) derived a thermally related surface rainfall budget through the combination of cloud budget with heat budget. In this chapter, precipitation efficiency is defined from the thermally related surface rainfall budget (*PEH*) and is calculated using the data from the two-dimensional (2D) cloud-resolving model simulations of a pre-summer torrential rainfall event over southern China in June 2008 (Wang et al., 2010; Shen et al., 2011a, 2011b) and is compared with the precipitation efficiency defined from water vapor related surface rainfall budget (Sui et al., 2007) to study the efficiency in thermodynamic aspect of the pre-summer heavy rainfall system.

The impacts of ice clouds on the development of convective systems have been intensively studied through the analysis of cloud-resolving model simulations (e.g., Yoshizaki, 1986;

Nicholls, 1987; Fovell and Ogura, 1988; Tao and Simpson, 1989; McCumber et al., 1991; Tao et al., 1991; Liu et al., 1997; Grabowski et al., 1999; Wu et al., 1999; Li et al., 1999; Grabowski and Moncrieff, 2001; Wu, 2002; Grabowski, 2003; Gao et al., 2006; Ping et al., 2007). Wang et al. (2010) studied microphysical and radiative effects of ice clouds on a pre-summer heavy rainfall event over southern China during 3-8 June 2008 through the analysis of sensitivity experiments and found that microphysical and radiative effects of ice clouds play equally important roles in the pre-summer heavy rainfall event. The total exclusion of ice microphysics decreased model domain mean surface rain rate primarily through the weakened convective rainfall caused by the exclusion of radiative effects of ice clouds in the onset phase and through the weakened stratiform rainfall caused by the exclusion of ice microphysical effects in the development and mature phases, whereas it increased the mean rain rate through the enhanced convective rainfall caused by the exclusion of ice microphysical effects in the decay phase. Thus, effects of ice clouds on precipitation efficiencies are examined through the analysis of the pre-summer heavy rainfall event in this chapter. Precipitation efficiency is defined in section 2. Pre-summer heavy rainfall event, model, and sensitivity experiments are described in section 3. The control experiment is discussed in section 4. Radiative and microphysical effects of ice clouds on precipitation efficiency and associated rainfall processes are respectively examined in sections 5 and 6. The conclusions are given in section 7.

2. Definitions of precipitation efficiency

The budgets for specific humidity (q_v), temperature (T), and cloud hydrometeor mixing ratio (q_l) in the 2D cloud resolving model used in this study can be written as

$$\frac{\partial q_v}{\partial t} = -\frac{\partial (u' q_v')}{\partial x} - \overline{u}^o \frac{\partial q_v'}{\partial x} - \overline{w}^o \frac{\partial q_v'}{\partial z} - w' \frac{\partial \overline{q}_v}{\partial z} - \frac{1}{\overline{\rho}} \frac{\partial}{\partial z} \overline{\rho w' q_v'} - S_{qv} - \overline{u}^o \frac{\partial \overline{q}_v}{\partial x} - \overline{w}^o \frac{\partial \overline{q}_v}{\partial z} \quad (1a)$$

$$\frac{\partial T}{\partial t} = -\frac{\partial}{\partial x}(\overline{u}^o + u')T' - \pi \overline{u}^o \frac{\partial \overline{\theta}^o}{\partial x} - \pi \overline{w}^o \frac{\partial}{\partial z}(\overline{\theta} + \theta') - \pi w' \frac{\partial \overline{\theta}}{\partial z} - \frac{\pi}{\overline{\rho}} \frac{\partial}{\partial z}(\overline{\rho} w' \theta') + \frac{Q_{cn}}{c_p} + \frac{Q_R}{c_p} \quad (1b)$$

$$\frac{\partial q_l}{\partial t} = -\frac{\partial (u q_l)}{\partial x} - \frac{1}{\overline{\rho}} \frac{\partial}{\partial z} \overline{\rho w q_l} + \frac{1}{\overline{\rho}} \frac{\partial}{\partial z} \overline{\rho}(w_{Tr} q_r + w_{Ts} q_s + w_{Tg} q_g) + S_{qv} \quad (1c)$$

where

$$S_{qv} = P_{CND} + P_{DEP} + P_{SDEP} + P_{GDEP} - P_{REVP} - P_{MLTS} - P_{MLTG} \quad (2a)$$

$$Q_{cn} = L_v S_{qv} + L_f P_{18} \quad (2b)$$

θ is potential temperature; u and w are zonal and vertical components of wind, respectively; ρ is air density that is a function of height; c_p is the specific heat of dry air at constant pressure; L_v, L_s, and L_f are latent heat of vaporization, sublimation, and fusion at T_o=0°C, respectively, L_s=L_v+L_f,; T_{oo}=-35 °C; and cloud microphysical processes in (2) can be found in Gao and Li (2008). Q_R is the radiative heating rate due to the convergence of net flux of solar and IR radiative fluxes. w_{Tr}, w_{Ts}, and w_{Tg} in (1c) are terminal velocities for raindrops, snow,

and graupel, respectively; overbar denotes a model domain mean; prime is a perturbation from model domain mean; and superscript ^{o} is an imposed observed value. The comparison between (1) and (2) shows that the net condensation term (S_{qv}) links water vapor, heat, and cloud budgets.

$$\begin{aligned} P_{18} &= P_{DEP} + P_{SDEP} + P_{GDEP} - P_{MLTS} - P_{MLTG} \\ &+ P_{SACW}(T < T_o) + P_{SFW}(T < T_o) + P_{GACW}(T < T_o) \\ &+ P_{IACR}(T < T_o) + P_{GACR}(T < T_o) + P_{SACR}(T < T_o) \\ &+ P_{GFR}(T < T_o) - P_{RACS}(T > T_o) - P_{SMLT}(T > T_o) \\ &- P_{GMLT}(T > T_o) + P_{IHOM}(T < T_{oo}) - P_{IMLT}(T > T_o) \\ &+ P_{IDW}(T_{oo} < T < T_o), \end{aligned} \tag{2c}$$

Following Gao et al. (2005) and Sui and Li (2005), the cloud budget (1c) and water vapor budget (1a) are mass integrated and their budgets can be, respectively, written as

$$P_S - Q_{CM} = Q_{WVS} = Q_{WVOUT} + Q_{WVIN} \tag{3}$$

$$Q_{WVT} + Q_{WVF} + Q_{WVE} = Q_{WVS} \tag{4}$$

where

$$P_S = P_r + P_s + P_g \tag{5a}$$

$$P_r = \overline{\rho} w_{Tr} q_r \,|_{z=0}, \tag{5b}$$

$$P_s = \overline{\rho} w_{Ts} q_s \,|_{z=0}, \tag{5c}$$

$$P_g = \overline{\rho} w_{Tg} q_g \,|_{z=0}, \tag{5d}$$

$$Q_{CM} = -\frac{\partial [q_l]}{\partial t} - [u \frac{\partial q_l}{\partial x}] - [w \frac{\partial q_l}{\partial z}] \tag{5e}$$

$$Q_{WVOUT} = [P_{CND}] + [P_{DEP}] + [P_{SDEP}] + [P_{GDEP}] \tag{5f}$$

$$Q_{WVIN} = -[P_{REVP}] - [P_{MLTG}] - [P_{MLTS}] \tag{5g}$$

$$Q_{WVT} = -\frac{\partial [q_v]}{\partial t} \tag{5h}$$

$$Q_{WVF} = -[\overline{u}^{o} \frac{\partial \overline{q}_v}{\partial x}] - [\overline{w}^{o} \frac{\partial \overline{q}_v}{\partial z}] - [\frac{\partial (u' q_v')}{\partial x}] - [\overline{u}^{o} \frac{\partial q_v'}{\partial x}] - [\overline{w}^{o} \frac{\partial q_v'}{\partial z}] - [w' \frac{\partial \overline{q}_v'}{\partial z}] \tag{5i}$$

$$Q_{WVE} = E_s \tag{5j}$$

Here, P_S is precipitation rate, and in the tropics, P_s=0 and P_g=0, P_S=P_r; E_s is surface evaporation; $[()] = \int_{z_b}^{z_t} \bar{\rho}()dz$, z_t and z_b are the heights of the top and bottom of the model atmosphere, respectively.

The heat budget (1b) is mass integrated and can be written as

$$S_{HT} + S_{HF} + S_{HS} + S_{LHLF} + S_{RAD} = Q_{WVS} \tag{6}$$

where

$$S_{HT} = \frac{c_p}{L_v}\frac{\partial [T]}{\partial t} \tag{7a}$$

$$S_{HF} = \frac{c_p}{L_v}[\frac{\partial}{\partial x}(\bar{u}^o + u')T' + \pi\bar{u}^o\frac{\partial \bar{\theta}^o}{\partial x} + \pi\bar{w}^o\frac{\partial}{\partial z}(\bar{\theta} + \theta') + \pi w'\frac{\partial \bar{\theta}}{\partial z}] \tag{7b}$$

$$S_{HS} = -\frac{c_p}{L_v}H_s \tag{7c}$$

$$S_{LHLF} = -\frac{L_f}{L_v} < P_{18} > \tag{7d}$$

$$S_{RAD} = -\frac{1}{L_v} < Q_R > \tag{7f}$$

H_s is surface sensible heat flux.

The equations (3), (4), and (6) indicate that the surface rain rate (P_S) is associated with favorable environmental water vapor and thermal conditions through cloud microphysical processes (Q_{WVOUT}+Q_{WVIN}). Following Gao and Li (2010), the cloud budget (3) and water vapor budget (4) are combined by eliminating Q_{WVOUT}+Q_{WVIN} to derive water vapor related surface rainfall equation (P_{SWV}),

$$P_{SWV}=Q_{WVT}+Q_{WVF}+Q_{WVE}+Q_{CM} \tag{8a}$$

In (8a), the surface rain rate (P_{SWV}) is associated with local atmospheric drying (Q_{WVT} >0)/moistening (Q_{WVT} <0), water vapor convergence (Q_{WVF} >0)/divergence (Q_{WVF} <0), surface evaporation (Q_{WVE}), and decrease of local hydrometeor concentration/hydrometeor convergence (Q_{CM} >0) or increase of local hydrometeor concentration/hydrometeor divergence (Q_{CM} <0). Similarly, the cloud budget (3) and heat budget (6) are combined by eliminating Q_{WVOUT}+Q_{WVIN} to derive thermally related surface rainfall equation (P_{SH}),

$$P_{SH}=S_{HT}+S_{HF}+S_{HS}+S_{LHLF}+S_{RAD}+Q_{CM}. \tag{8b}$$

In (8b), the surface rain rate (P_{SH}) is related to local atmospheric warming (S_{HT} >0)/cooling (S_{HT} <0), heat divergence (S_{HF} >0)/convergence (S_{HF} <0), surface sensible heat (S_{HS}), latent heat due to ice-related processes (S_{LHLF}), radiative cooling (S_{RAD} >0)/heating (S_{RAD} <0), and

decrease of local hydrometeor concentration/hydrometeor convergence (Q_{CM} >0) or increase of local hydrometeor concentration/hydrometeor divergence (Q_{CM} <0). P_{SWV} = P_{SH} = P_S.

From (8), precipitation efficiencies can be respectively defined as

$$PEWV = \frac{P_S}{\sum_{i=1}^{4} H(Q_i)Q_i} \tag{7a}$$

$$PEH = \frac{P_S}{\sum_{i=1}^{5} H(S_i)S_i + H(Q_{CM})Q_{CM}} \tag{7b}$$

where Q_i=(Q_{WVT}, Q_{WVF}, Q_{WVE}, Q_{CM}); S_i=(S_{HT}, S_{HF}, S_{HS}, S_{LHLF}, S_{RAD}); H is the Heaviside function, $H(F)$=1 when F>0, and $H(F)$=0 when $F \leq 0$. Large-scale heat precipitation efficiency (*PEH*) is first introduced in this study, whereas large-scale water vapor precipitation efficiency (*PEWV*) is exactly same to *LSPE2* defined by Sui et al. (2007).

3. Pre-summer rainfall case, model, and experiments

The pre-summer rainy season is the major rainy season over southern China, in which the rainfall starts in early April and reaches its peak in June (Ding, 1994). Although the rainfall is a major water resource in annual water budget, the torrential rainfall could occur during the pre-summer rainfall season and can lead to tremendous property damage and fatalities. In 1998, for instance, the torrential rainfall resulted in over 30 billion USD in damage and over 100 fatalities. Thus, many observational analyses and numerical modeling have been contributed to understanding of physical processes responsible for the development of pre-summer torrential rainfall (e.g., Krishnamurti et al., 1976; Tao and Ding, 1981; Wang and Li, 1982; Ding and Murakami, 1994; Simmonds et al., 1999). Recently, Wang et al. (2010) and Shen et al. (2011a, 2011b) conducted a series of sensitivity experiments of the pre-summer torrential rainfall occurred in the early June 2008 using 2D cloud-resolving model and studied effects of vertical wind shear, radiation, and ice clouds on the development of torrential rainfall. They found that these effects on torrential rainfall are stronger during the decay phase than during the onset and mature phases. During the decay phase of convection on 7 June 2008, the increase in model domain mean surface rain rate resulting from the exclusion of vertical wind shear is associated with the slowdown in the decrease of perturbation kinetic energy due to the exclusion of barotropic conversion from mean kinetic energy to perturbation kinetic energy. The increase in domain-mean rain rate resulting from the exclusion of cloud radiative effects is related to the enhancement of condensation and associated latent heat release as a result of strengthened radiative cooling. The increase in the mean surface rain rate is mainly associated with the increase in convective rainfall, which is in turn related to the local atmospheric change from moistening to drying. The increase in mean rain rate caused by the exclusion of ice clouds results from the increases in the mean net condensation and mean latent heat release caused by the strengthened mean radiative cooling associated with the removal of radiative effects of ice clouds. The increase

in mean rain rate caused by the removal of radiative effects of water clouds corresponds to the increase in the mean net condensation.

The pre-summer torrential rainfall event studied by Wang et al. (2010) and Shen et al. (2011a, 2011b) will be revisited to examine the thermodynamic aspects of precipitation efficiency and effects of ice clouds on precipitation efficiency. The cloud-resolving model (Soong and Ogura, 1980; Soong and Tao, 1980; Tao and Simpson, 1993) used in modeling the pre-summer torrential rainfall event in Wang et al. (2010) is the 2D version of the model (Sui et al., 1994, 1998) that was modified by Li et al. (1999). The model is forced by imposed large-scale vertical velocity and zonal wind and horizontal temperature and water vapor advections, which produces reasonable simulation through the adjustment of the mean thermodynamic stability distribution by vertical advection (Li et al., 1999). The modifications by Li et al. (1999) include: (1) the radius of ice crystal is increased from 50μm (Hsie et al., 1980) to 100μm (Krueger et al., 1995) in the calculation of growth of snow by the deposition and riming of cloud water, which yields a significant increase in cloud ice; (2) the mass of a natural ice nucleus is replaced by an average mass of an ice nucleus in the calculation of the growth of ice clouds due to the position of cloud water; (3) the specified cloud single scattering albedo and asymmetry factor are replaced by those varied with cloud and environmental thermodynamic conditions. Detailed descriptions of the model can be found in Gao and Li (2008). Briefly, the model includes prognostic equations for potential temperature and specific humidity, prognostic equations for hydrometeor mixing ratios of cloud water, raindrops, cloud ice, snow, and graupel, and perturbation equations for zonal wind and vertical velocity. The model uses the cloud microphysical parameterization schemes (Lin et al., 1983; Rutledge and Hobbs, 1983, 1984; Tao et al., 1989; Krueger et al., 1995) and solar and thermal infrared radiation parameterization schemes (Chou et al., 1991, 1998; Chou and Suarez, 1994). The model uses cyclic lateral boundaries, and a horizontal domain of 768 km with 33 vertical levels, and its horizontal and temporal resolutions are 1.5 km and 12 s, respectively.

The data from Global Data Assimilation System (GDAS) developed by the National Centers for Environmental Prediction (NCEP), National Oceanic and Atmospheric Administration (NOAA), USA are used to calculate the forcing data for the model over a longitudinally oriented rectangular area of 108-116^{o}E, 21-22^{o}N over coastal areas along southern Guangdong and Guangxi Provinces and the surrounding northern South China Sea. The horizontal and temporal resolutions for NCEP/GDAS products are 1^{o}x1^{o} and 6 hourly, respectively. The model is imposed by large-scale vertical velocity, zonal wind (Fig. 1), and horizontal temperature and water vapor advections (not shown) averaged over 108-116^{o}E, 21-22^{o}N. The model is integrated from 0200 Local Standard Time (LST) 3 June to 0200 LST 8 June 2008 during the pre-summer heavy rainfall. The surface temperature and specific humidity from NCEP/GDAS averaged over the model domain are uniformly imposed on each model grid to calculate surface sensible heat flux and evaporation flux. The 6-hourly zonally-uniform large-scale forcing data are linearly interpolated into 12-s data, which are uniformly imposed zonally over model domain at each time step. The imposed large-scale vertical velocity shows the gradual increase of upward motions from 3 June to 6 June. The maximum upward motion of 18 cm s^{-1} occurred around 9 km in the late morning of 6 June. The upward motions decreased dramatically on 7 June. The lower-tropospheric westerly winds of 4 - 12 m s^{-1} were maintained during the rainfall event.

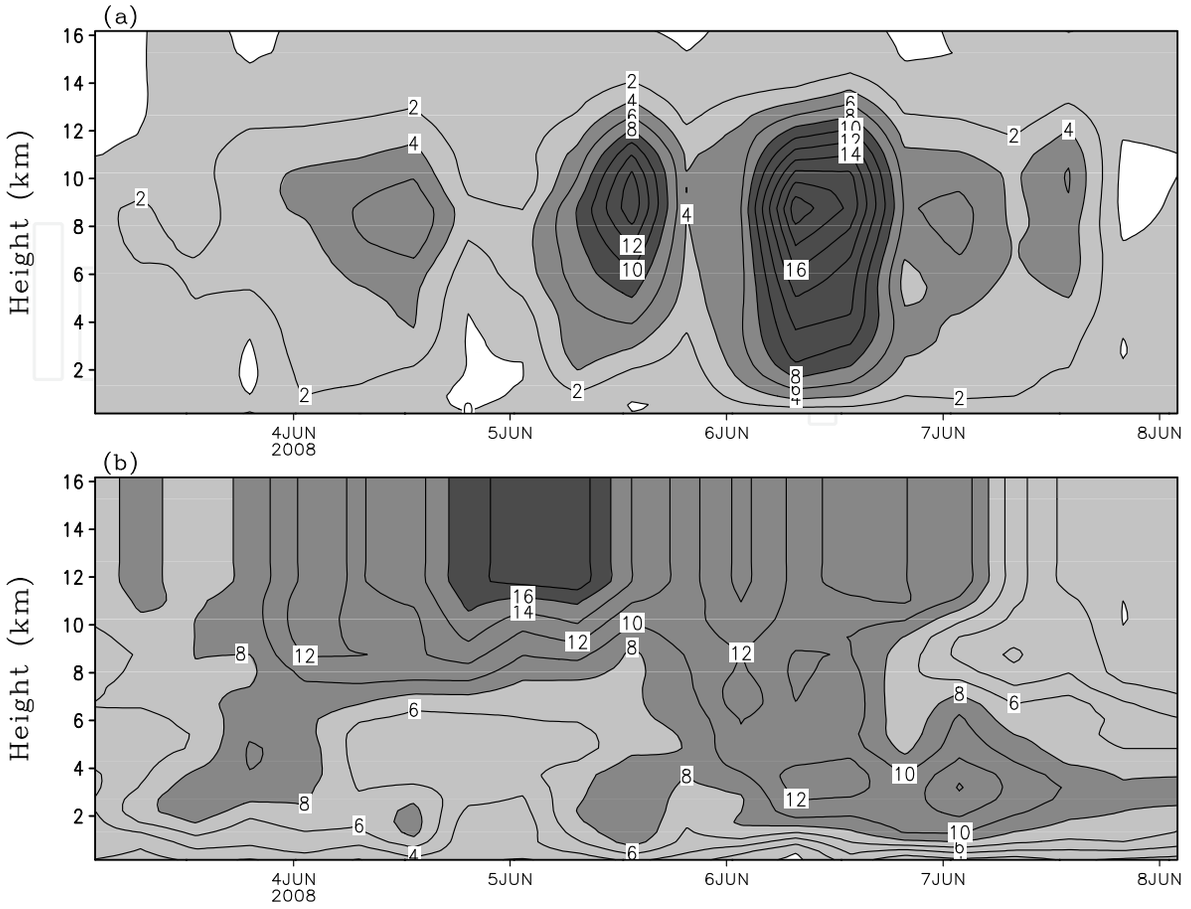

Fig. 1. Temporal and vertical distribution of (a) vertical velocity (cm s^{-1}) and (b) zonal wind (m s^{-1}) from 0200 LST 3 June – 0200 LST 8 June 2008. The data are averaged in a rectangular box of 108-116°E, 21-22°N from NCEP/GDAS data. Ascending motion in (a) and westerly wind in (b) are shaded.

In the control experiment (C), the model is integrated with the initial vertical profiles of temperature and specific humidity from NCEP/GDAS at 0200 LST 3 June 2008. The model is integrated with the initial conditions and constant large-scale forcing at 0200 LST 3 June for 6 hours during the model spin-up period and the 6-hour model data are not used for analysis. The comparison in surface rain rate between the simulation and rain gauge observation averaged from 17 stations over southern Guangdong and Guangxi reveals a fair agreement with a gradual increase from 3-6 June and a rapid decrease from 6-7 June (Fig. 2). Their RMS difference (0.97 mm h^{-1}) is significantly smaller than the standard derivations of simulated (1.22 mm h^{-1}) and observed (1.26 mm h^{-1}) rain rates. The differences in surface rain rate between the simulation and observation can reach 2 mm h^{-1}, as seen in the previous studies (e.g., Li et al., 1999; Xu et al., 2007; Wang et al., 2009). The differences may partially be from the comparison of small hourly local sampling of rain gauge observations over 35% of model domain over land and no rain gauge observations over 65% of model domain over ocean with large model domain averages of model data in the control experiment with imposed 6-hourly large-scale forcing. The convection may be affected by land-ocean contrast and orography; these effects are included in the large-scale forcing imposed in the model.

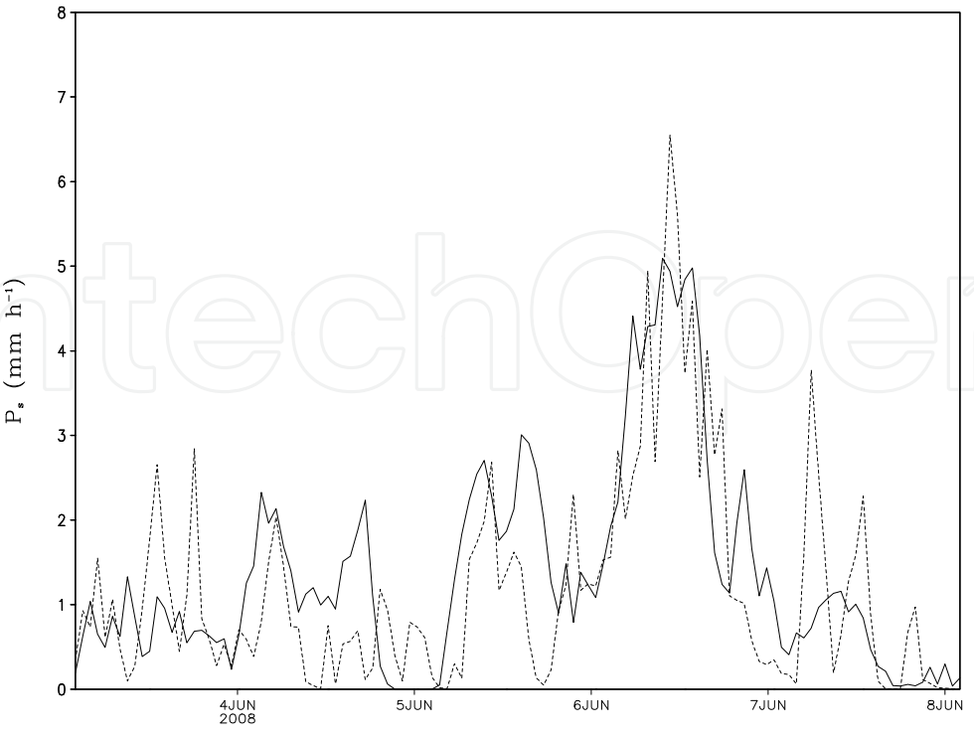

Fig. 2. Time series of surface rain rates (mm h^{-1}) simulated in the control experiment (solid) and from rain gauge observation (dash).

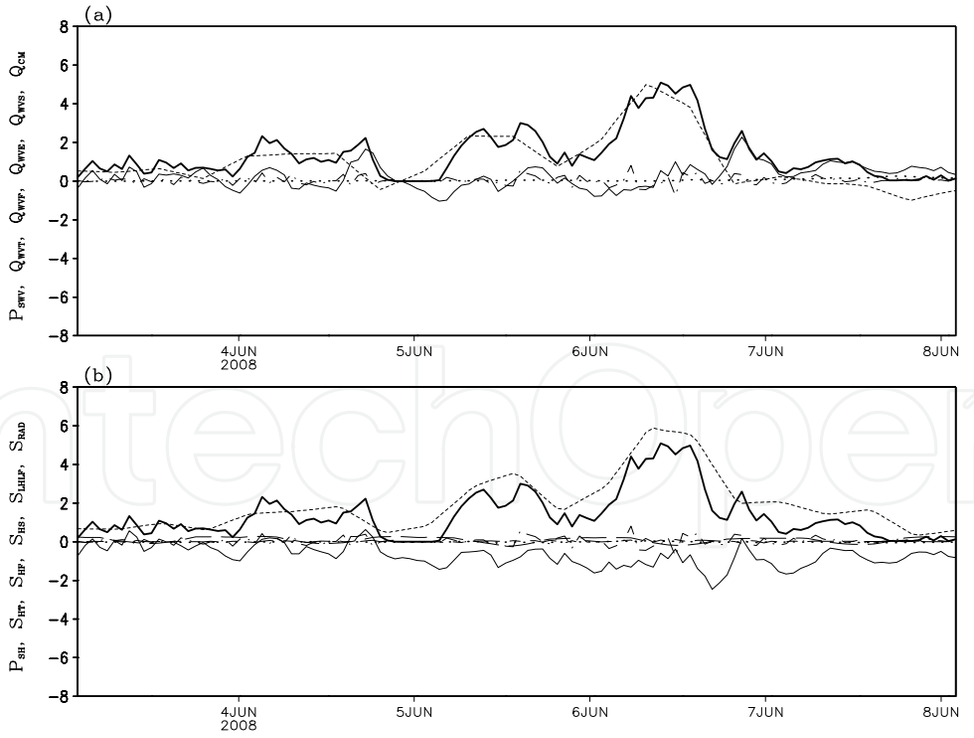

Fig. 3. Time series of model domain means of (a) P_{SWV} (dark solid), Q_{WVT} (light solid), Q_{WVF} (short dash), Q_{WVE} (dot), Q_{CM} (dot dash), and (b) P_{SH} (dark solid), S_{HT} (light solid), S_{HF} (short dash), S_{HS} (dot), S_{LHLF} (long short dash), S_{RAD} (long dash), and Q_{CM} (dot dash) in C. Unit is mm h^{-1}.

To investigate effects of ice clouds on precipitation efficiency, two sensitivity experiments are examined in this study. Experiment CNIR is identical to C except that the mixing ratios of ice hydrometeor are set to zero in the calculation of radiation. Experiment CNIR is compared with C to study radiative effects of ice clouds on rainfall responses to the large-scale forcing. Experiment CNIM is identical to C except in CNIM ice clouds (the ice hydrometeor mixing ratio and associated microphysical processes) are excluded. The comparison between CNIM and CNIR reveals impacts of the removal of microphysical efficient of ice clouds on rainfall responses to the large-scale forcing in the absence of radiative effects of ice clouds. The hourly model simulation data are used in the following discussions of this study.

4. The control experiment: C

Model domain mean surface rain rate starts on 3 June 2008 with the magnitude of about 1 mm h^{-1} (Fig. 3), which corresponds to the weak upward motions with a maximum of 2 cm s^{-1} at 6-8 km (Fig. 1a). The rain rate increases to 2 mm h^{-1} as the upward motions increase up to over 6 cm s^{-1} on 4 June. When the upward motions weaken in the evening of 4 June and a weak downward motion occurs near the surface, the mean rainfall vanishes. As upward motions pick their strengths on 5 June, the mean rain rate intensifies (over 2 mm h^{-1}). The mean rainfall reaches its peak on 6 June (over 4 mm h^{-1}) as the upward motions have a maximum of over 20 cm s^{-1}. The upward motions rapidly weaken on 7 June, which leads to the significant reduction in the mean rainfall. Thus, four days (4, 5, 6, and 7 June) are defined as the onset, development, mature, and decay phases of the rainfall event, respectively. During 3-6 June, the mean rainfall is mainly associated with the mean water vapor convergence ($Q_{WVF}>0$) in water vapor related surface rainfall budget and the mean heat divergence ($S_{HF}>0$) in thermally related surface rainfall budget. Local atmospheric drying ($Q_{WVT}>0$) and moistening ($Q_{WVT}<0$) occur while the mean local atmospheric cooling ($S_{HT}<0$) prevails. The mean hydrometeor loss/convergence (Q_{CM}) has small hourly fluctuations. The mean radiative heating during the daytime and mean radiative cooling during the nighttime have the much smaller magnitudes than the mean heat divergence and the mean local heat change do in thermally related surface rainfall budget. On 7 June, the mean water vapor related surface rainfall budget shows that the rainfall is associated with local atmospheric drying while water vapor divergence prevails. The mean thermally related surface rainfall budget reveals that the rainfall is related to heat divergence while the heat divergence cools local atmosphere.

The calculation of precipitation efficiency using model domain mean model simulation data shows that *PEWV* generally is higher than *PWH* (Fig. 4a) because the rainfall source from the mean water vapor convergence in water vapor related surface rainfall budget is weaker than the rainfall source from the mean heat divergence in thermally related surface rainfall budget (Fig. 3). This suggests that the precipitation system is more efficient in the consumption of rainfall source from water vapor than in the consumption of the rainfall source from heat. The root-mean-squared (RMS) difference between *PEWV* and *PEH* is 24.4%. Both *PEWV* and *PEH* generally increase as surface rain rate increases (Fig. 5a). This indicates that the precipitation system generally is more efficient for high surface rain rates than for low surface rain rates. The ranges of *PEWV* and *PEH* are smaller when surface rain rate is higher than 3 mm h^{-1} (70-100%) than when surface rain rate is lower than 3 mm h^{-1} (0-100%).

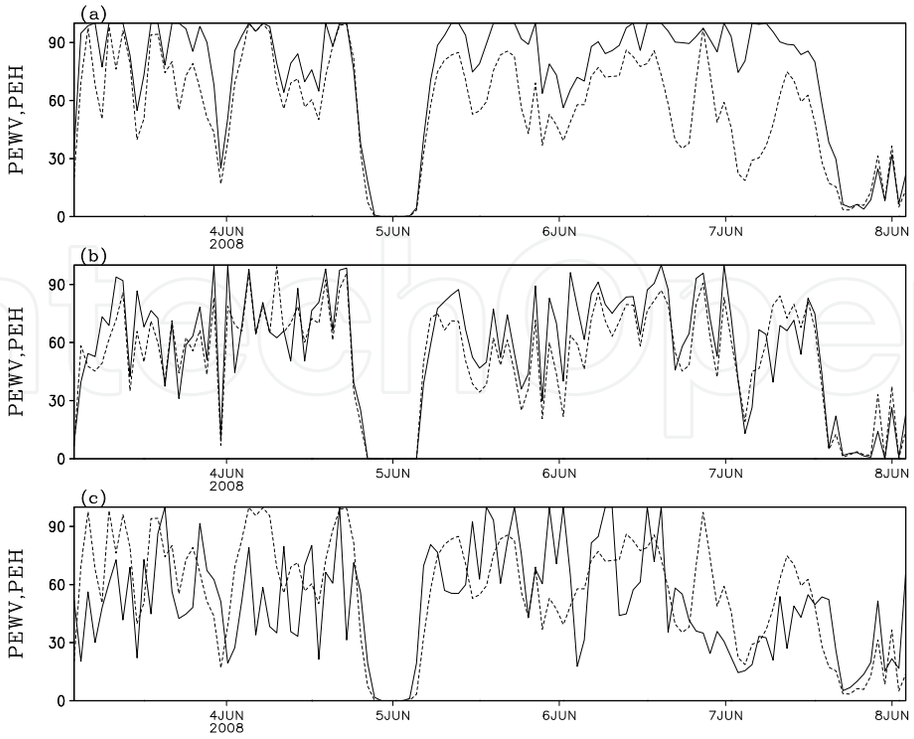

Fig. 4. Time series of *PEWV* (solid) and *PEH* (dash) calculated using (a) model domain mean data and data from (b) convective and (c) raining stratiform regions in C. Unit is %.

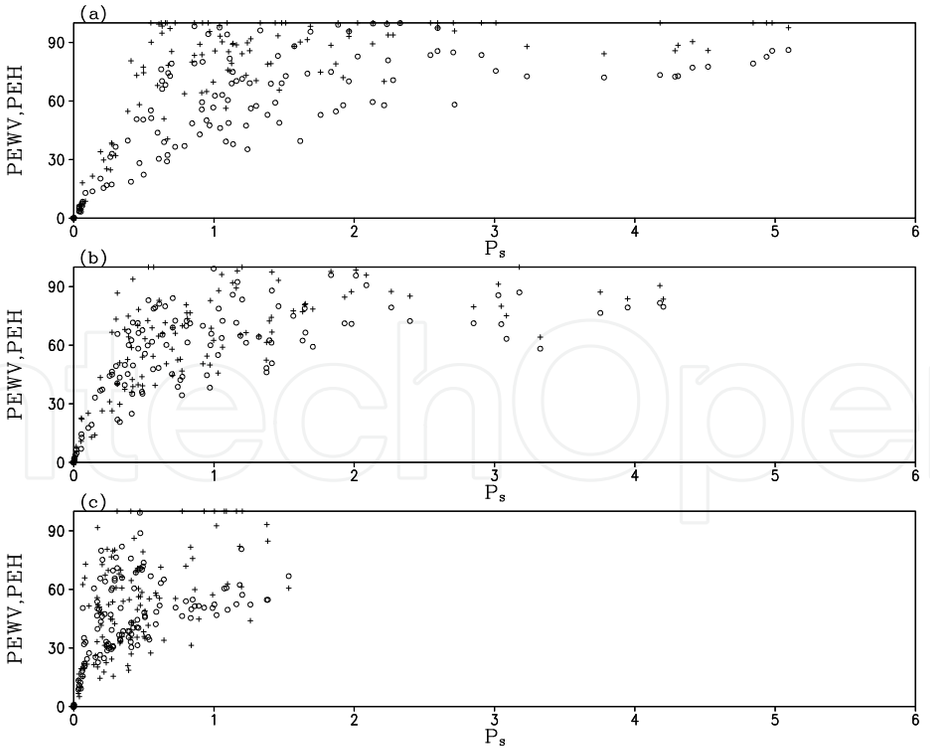

Fig. 5. *PEWV* versus P_S (cross) and *PEH* versus P_S (open circle) calculated using (a) model domain mean data and data from (b) convective and (c) raining stratiform regions in C. Units are % for *PEWV* and *PEH* and mm h^{-1} for P_S.

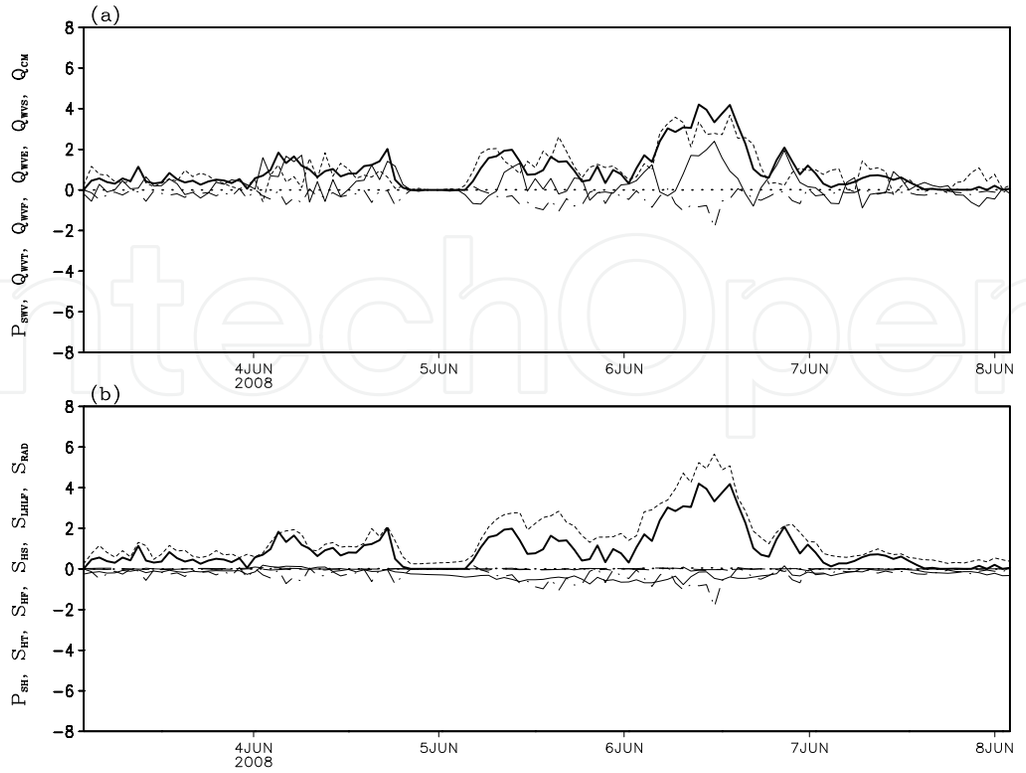

Fig. 6. Time series of contributions of model domain mean of (a) P_{SWV} (dark solid), Q_{WVT} (light solid), Q_{WVF} (short dash), Q_{WVE} (dot), Q_{CM} (dot dash), and (b) P_{SH} (dark solid), S_{HT} (light solid), S_{HF} (short dash), S_{HS} (dot), S_{LHLF} (long short dash), S_{RAD} (long dash), and Q_{CM} (dot dash) from convective regions in C. Unit is mm h^{-1}.

Model domain mean surface rainfall consists of convective and stratiform rainfall. Convective rainfall differs from stratiform rainfall in four ways. First, convective rain rates are higher than stratiform rain rates. Second, convective rainfall is associated with stronger horizontal reflectivity gradients than stratiform rainfall. Third, upward motions associated with convective rainfall are much stronger than those associated with stratiform rainfall. Fourth, the accretion of cloud water by raindrops via collisions in strong updraft cores and the vapor deposition on ice particles are primary microphysical processes that are responsible for the development of convective and stratiform rainfall,respectively (Houghton 1968). The convective-stratiform rainfall partitioning scheme used in this study is developed by Tao and Simpson (1993) and modified by Sui et al. (1994). This scheme partitions each vertical column containing clouds in 2-D x-z framework into convective or stratiform based on the following criterion. Model grid point is identified as convective if it has a rain rate twice as large as the average taken over the surrounding four grid points, the one grid point on either side of this grid point, and any grid point with a rain rate of 20 mm h^{-1} or more. All non-convective cloudy points are considered as stratiform. In addition, grid points over stratiform regions are further checked and identified as convective when following conditions are met. Over raining stratiform regions, cloud water below the melting level is greater than 0.5 g kg^{-1} or the maximum updraft above 600 hPa exceeds 5 m s^{-1}, or over non-raining stratiform regions, cloud water mixing ratio of 0.025 g kg^{-1} or more exists or the maximum updraft exceeds 5 m s^{-1} below the melting level.

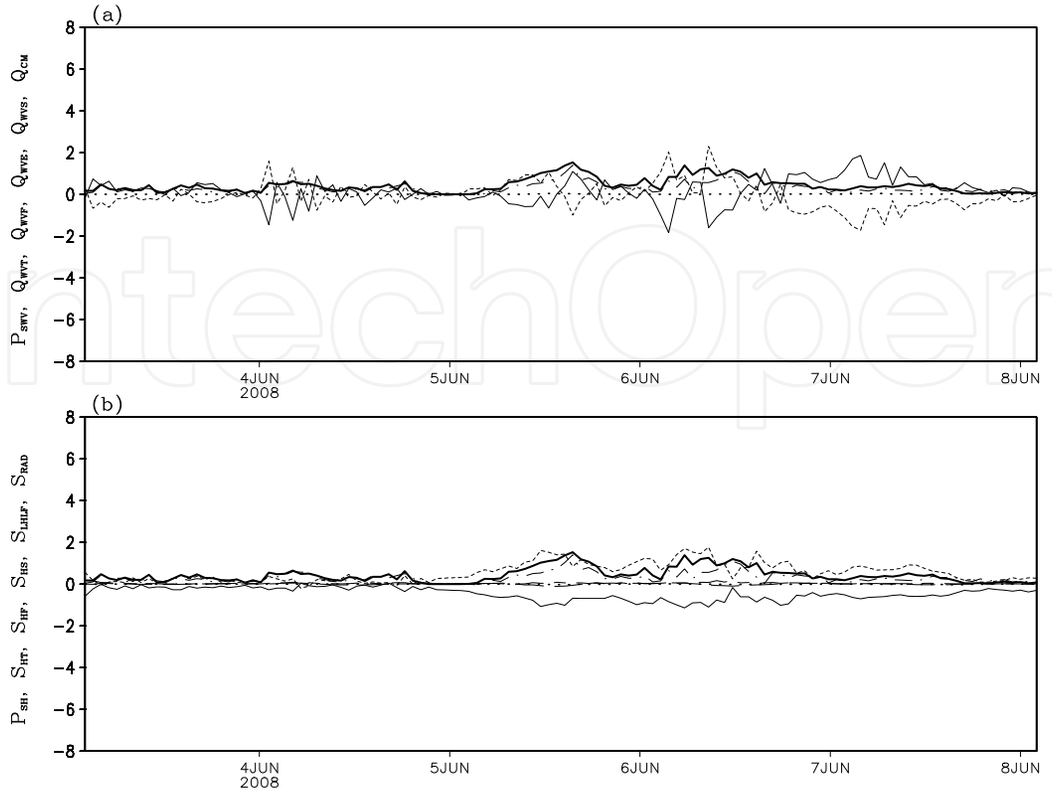

Fig. 7. Time series of contributions of model domain mean of (a) P_{SWV} (dark solid), Q_{WVT} (light solid), Q_{WVF} (short dash), Q_{WVE} (dot), Q_{CM} (dot dash), and (b) P_{SH} (dark solid), S_{HT} (light solid), S_{HF} (short dash), S_{HS} (dot), S_{LHLF} (long short dash), S_{RAD} (long dash), and Q_{CM} (dot dash) from raining stratiform regions in C. Unit is mm h^{-1}.

Convective rain rate (Fig. 6) is much higher than stratiform rain rate (Fig. 7) and mainly accounts for model domain mean surface rain rate (Fig. 3). Over convective regions, rainfall is associated with water vapor convergence in water vapor related surface rainfall budget (Fig. 6a) and heat divergence in thermally related surface rainfall budget (Fig. 6b). Q_{CM} is negative over convective regions whereas Q_{CM} is positive over raining stratiform regions (Fig. 8), which indicates the transport of hydrometeor concentration from convective regions (Q_{CM}<0) to raining stratiform regions (Q_{CM}>0). The hydrometeor transport is associated with the local atmospheric drying (Q_{WVT}>0) over convective regions because Q_{WVT} and Q_{CM} have similar magnitudes but opposite signs. The water vapor convergence, local atmospheric drying, and heat divergence are the rainfall sources whereas the local atmospheric cooling and the transport of hydrometeor concentration from convective regions to raining stratiform regions are the rainfall sinks. *PEWV* generally is higher than *PEH* (Fig. 4b) because the rainfall source from water vapor convergence in water vapor related surface rainfall budget is weaker than the rainfall source from heat divergence in thermally related surface rainfall budget (Fig. 6). *PEWV* is lower than *PEH* on 4 and 7 June because the rainfall source from water vapor convergence is stronger than the rainfall source from heat divergence. The RMS difference between *PEWV* and *PEH* is 12.5%. Both *PWEV* and *PEH* increase as convective rainfall intensifies (Fig. 5b). Precipitation efficiency ranges from 60% to 90% as convective rain rate is higher than 2 mm h^{-1}, whereas it ranges from 0 to 100% as convective rain rate is lower than 2 mm h^{-1}.

Over raining stratiform regions, rainfall is primarily associated with the transport of hydrometeor concentration from convective regions to raining stratiform regions because water vapor divergence dries local atmosphere on 3 and 7 June and water vapor convergence moistens local atmosphere on 4-6 June and heat divergence cools local atmosphere (Fig. 7). *PWH* is generally higher than *PEWV* on 3, 4, and 7 June whereas it is generally lower than *PEWV* on 5-6 June (Fig. 4c). The RMS difference between *PEWV* and *PEH* is 23.8%, which largely accounts for the RMS difference in the model domain mean calculations. The ranges of precipitation efficiencies for the surface rain rate of lower than 1 mm h^{-1} (0-100%) are larger than those for the surface rain rate of higher than 1 mm h^{-1} (45-100%).

5. Radiative effects of ice clouds: CNIR versus C

The calculations of model domain mean simulation data show that *PEWV* is insensitive to radiative effects of ice clouds on 4 June, whereas the exclusion of radiative effects of ice clouds decreases *PEH* (Table 1). The removal of radiative effects of ice clouds increases *PEWV,* but it barely affects *PEH* on 5 June. The elimination of radiative effects of ice clouds decreases *PEWV* and *PEH* on 6 June. The exclusion of radiative effects of ice clouds increases *PEWV* but it decreases *PEH* on 7 June. On 4 June, the water vapor realted surface rainfall budgets reveal that all rainfall processes contribute to rain rate in C and CNIR (Table 2), which leads to 100% of *PEWV* in the two experiments. The thermally related surface rainfall budgets show that rainfall is associated with heat divergence and radiative cooling in the two experiments (Table 3). Thus, local atmospheric cooling (S_{HT}<0) makes PEH less than 100% in the two experiments.

(a)	Model domain mean			Convective regions			Raining stratiform regions		
	C	CNIR	CNIM	C	CNIR	CNIM	C	CNIR	CNIM
4 June	100.0	100.0	91.5	77.8	68.8	83.0	82.3	66.7	58.3
5 June	92.0	98.4	81.0	71.5	70.3	80.6	100.0	90.8	100.0
6 June	99.8	96.3	91.3	81.9	80.5	87.3	100.0	82.2	100.0
7 June	62.8	64.6	60.4	55.0	67.2	77.2	28.1	36.8	51.5

(b)	Model domain mean			Convective regions			Raining stratiform regions		
	C	CNIR	CNIM	C	CNIR	CNIM	C	CNIR	CNIM
4 June	77.0	72.0	68.5	73.5	64.1	77.0	65.2	67.5	47.0
5 June	63.3	63.8	57.0	52.1	51.5	56.5	47.3	47.1	34.4
6 June	71.9	69.3	68.7	70.6	69.4	77.6	49.1	43.7	34.3
7 June	36.7	35.1	34.2	48.6	49.2	49.4	33.4	28.2	29.1

Table 1. (a) *PEWV* and (b) *PEH* calculated data averaged daily and over model domain, convective regions, and raining stratiform regions in C, CNIR, and CNIM. Unit is %.

		Model domain mean			Convective regions			Raining stratiform regions		
		C	CNIR	CNIM	C	CNIR	CNIM	C	CNIR	CNIM
4 June	P_{SWV}	1.16	1.07	0.92	0.86	0.73	0.80	0.30	0.34	0.13
	Q_{WVT}	0.22	0.19	0.16	0.52	0.46	0.31	-0.06	-0.17	-0.09
	Q_{WVF}	0.87	0.86	0.84	0.57	0.60	0.64	0.09	0.18	0.13
	Q_{WVE}	0.01	0.01	0.01	0.00	0.00	0.00	0.00	0.00	0.00
	Q_{CM}	0.05	0.01	-0.09	-0.24	-0.33	-0.16	0.28	0.32	0.09
5 June	P_{SWV}	1.54	1.59	1.27	0.92	0.99	0.93	0.62	0.59	0.35
	Q_{WVT}	-0.13	-0.03	-0.17	0.10	0.35	0.21	0.00	-0.06	0.10
	Q_{WVF}	1.59	1.53	1.55	1.17	1.06	0.93	0.20	0.19	0.13
	Q_{WVE}	0.03	0.04	0.02	0.00	0.01	0.00	0.01	0.02	0.00
	Q_{CM}	0.05	0.04	-0.13	-0.37	-0.42	-0.22	0.41	0.44	0.12
6 June	P_{SWV}	2.95	2.84	2.69	2.21	2.21	2.36	0.74	0.64	0.32
	Q_{WVT}	0.34	0.41	0.31	0.77	0.92	0.87	0.03	-0.14	0.17
	Q_{WVF}	2.57	2.51	2.62	1.92	1.80	1.83	0.23	0.38	0.03
	Q_{WVE}	0.04	0.04	0.02	0.01	0.01	0.00	0.01	0.02	0.00
	Q_{CM}	-0.01	-0.11	-0.26	-0.49	-0.53	-0.34	0.47	0.38	0.12
7 June	P_{SWV}	0.54	0.51	0.46	0.29	0.33	0.32	0.25	0.19	0.15
	Q_{WVT}	0.64	0.59	0.67	-0.09	0.08	0.08	0.65	0.30	0.19
	Q_{WVF}	-0.32	-0.28	-0.23	0.52	0.39	0.32	-0.63	-0.32	-0.14
	Q_{WVE}	0.16	0.17	0.10	0.01	0.01	0.00	0.02	0.04	0.01
	Q_{CM}	0.05	0.03	-0.08	-0.15	-0.16	-0.09	0.20	0.17	0.09

Table 2. Water vapor related surface rainfall budget (P_{SWV}, Q_{WVT}, Q_{WVF}, Q_{WVE}, and Q_{CM}) averaged daily and over model domain, convective regions, and raining stratiform regions in C, CNIR, and CNIM. Unit is mm h^{-1}.

The removal of radiative effects of ice clouds decreases *PEH* from C to CNIR through the enhanced local atmospheric cooling associated with the enhanced radiative cooling because of similar heat divergence in the two experiments. On 5 June, the elimination of radiative effects of ice clouds increases *PEWV* through the reduced local atmospheric moistening (Q_{WVT}<0) associated with the decreased water vapor convergence (Q_{WVF}>0). The two experiments have similar *PEH* because of similar heat related rainfall processes. On 6 June, the exclusion of radiative effects of ice clouds decreases *PEWV* and *PEH* from C to CNIR through the enhanced hydrometeor gain (Q_{CM}>0) because water vapor and heat processes have similar contributions to rainfall ($Q_{WVT}+Q_{WVF}+Q_{WVE} \approx S_{HT}+S_{HF}+S_{HS}+S_{LHLF}+S_{RAD}$) in the two experiments. On 7 June, the removal of radiative effects of ice clouds increases *PEWV* through the decreased water vapor divergence, whereas it decreases *PEH* through the enhanced local atmospheric cooling associated with the enhanced radiative cooling.

Over convective regions, the exclusion of radiative effects of ice clouds decreases *PEWV* and *PEH* through the intensified transport of hydrometeor concentration from convective regions to raining stratiform regions (Q_{CM}<0) because water vapor and heat processes have similar contributions to rainfall in the two experiments on 4 June. Similar magnitudes of rainfall sources associated with water vapor, heat, and cloud processes lead to similar

PEWV and *PEH* on 5 and 6 June. On 7 June, the exclusion of radiative effects of ice clouds increases *PEWV* through the local atmospheric change from moistening in C to drying in CNIR associated with the decrease in water vapor convergence while the two experiments have similar transport rates of hydrometeor concentration from convective regions to raining stratiform regions. The two experiments have similar *PEH* because of similar thermal processes. Note that radiative cooling is negligibly small over convective regions.

Over raining stratiform regions, the removal of radiative effects of ice clouds decreases *PEWV* through the enhanced local atmospheric moistening on 4 June. Because the increase in rainfall from C to CNIR is similar to the increase in rainfall source that is from the heat divergence and the transport of hydrometeor concentration from convective regions to raining stratiform regions, the increase in stratiform rainfall from C to CNIR leads to the increase in *PEH*. On 5 June, the elimination of radiative effects of ice clouds decreases *PEWV* because the local water vapor is barely changed in C and the local atmospheric moistening occurs in CNIR. The two experiments have similar *PEH* due to similar rainfall sources from thermal and cloud processes. On 6 June, the exclusion of radiative effects of ice clouds leads to the decreases in *PEWV* through the local atmospheric change from drying in C to moistening in CNIR and reduces *PEH* through the enhanced local atmospheric cooling. On 7 June, the removal of radiative effects of ice clouds increases *PEWV* through the slowdown in water vapor divergence. Because the decrease in rainfall is similar to the decrease in the rainfall source from heat divergence and transport of hydrometeor concentration from convective regions to raining stratiform regions as a result of similar local atmospheric cooling rate in the two experiments, the decrease in stratiform rainfall from C to CNIR leads to the decrease in *PEH*.

6. Microphysical effects of ice clouds: CNIM versus CNIR

The calculations of model domain mean simulation data show the decreases in *PEWV* and *PEH* from CNIR to CNIM during the life span of pre-summer heavy rainfall event (Figs. 9a-10a). On 4 June, the exclusion of microphysical effects of ice clouds decreases *PEWV* and *PEH* through the hydrometeor change from loss in CNIR to gain in CNIM and the weakened local atmospheric cooling (Figs. 11a-17a). On 5 June, the decrease in *PEWV* is associated with the intensification in local atmospheric moistening and the hydrometeor change from loss in CNIR to gain in CNIM. The reduction in *PEH* is related to the hydrometeor change from loss in CNIR to gain in CNIM. On 6 June, the decrease in *PEWV* corresponds to the strengthened hydrometeor gain. *PEH* is barely changed in the two experiments because of similar rates of rainfall source from thermal processes. On 7 June, the decreases in *PEWV* and *PEH* result from the hydrometeor change from loss in CNIR to gain in CNIM although water vapor divergence and local atmospheric cooling are weakened.

Over convective regions, *PEWV* and *PEH* are increased from CNIR to CNIM during the life span of pre-summer heavy rainfall event (Figs. 9b-10b). The exclusion of microphysical effects of ice clouds increases *PEWV* and *PEH* through the weakened transport of hydrometeor concentration from convective regions to raining stratiform regions during 4-6 June (Figs. 11b-17b). The decrease in local atmospheric cooling also contributes to the increases in *PEWV* and *PEH* on 6 June. On 7 June, the removal of microphysical effects of ice clouds increases *PEWV* through the weakened transport of hydrometeor concentration from

convective regions to raining stratiform regions, whereas it barely changes *PEH* because of the offset between the weakened transport of hydrometeor concentration from convective regions to raining stratiform regions and the enhanced local atmospheric cooling (Figs. 14b and 15b).

		Model domain mean			Convective regions			Raining stratiform regions		
		C	CNIR	CNIM	C	CNIR	CNIM	C	CNIR	CNIM
4 June	P_{SH}	1.16	1.07	0.92	0.86	0.73	0.80	0.30	0.34	0.13
	S_{HT}	-0.34	-0.41	-0.33	-0.05	-0.06	-0.08	-0.16	-0.16	-0.14
	S_{HF}	1.30	1.28	1.24	1.15	1.11	1.02	0.15	0.14	0.18
	S_{HS}	-0.01	-0.01	-0.01	0.01	0.00	0.00	0.00	0.00	0.00
	S_{LHLF}	0.02	0.00	0.00	-0.01	-0.02	0.00	0.03	0.02	0.00
	S_{RAD}	0.13	0.18	0.12	0.01	0.02	0.01	0.00	0.02	0.00
	Q_{CM}	0.05	0.01	-0.09	-0.24	-0.33	-0.16	0.28	0.32	0.09
5 June	P_{SH}	1.54	1.59	1.27	0.92	0.99	0.93	0.62	0.59	0.35
	S_{HT}	-0.88	-0.88	-0.82	-0.46	-0.48	-0.49	-0.68	-0.66	-0.65
	S_{HF}	2.30	2.28	2.14	1.76	1.91	1.63	0.88	0.74	0.89
	S_{HS}	-0.01	-0.02	-0.01	0.00	0.01	0.00	-0.01	-0.01	0.00
	S_{LHLF}	0.01	0.01	0.00	-0.01	-0.03	0.00	0.03	0.04	0.00
	S_{RAD}	0.07	0.16	0.09	0.00	0.01	0.01	-0.01	0.03	0.00
	Q_{CM}	0.05	0.04	-0.13	-0.37	-0.42	-0.22	0.41	0.44	0.12
6 June	P_{SH}	2.95	2.84	2.69	2.21	2.21	2.36	0.74	0.64	0.32
	S_{HT}	-1.15	-1.14	-0.97	-0.40	-0.40	-0.34	-0.76	-0.81	-0.62
	S_{HF}	4.00	3.92	3.81	3.10	3.15	3.02	0.98	1.00	0.82
	S_{HS}	0.00	-0.01	0.01	0.02	0.01	0.01	-0.01	-0.01	0.00
	S_{LHLF}	0.03	0.03	0.00	-0.03	-0.04	0.00	0.06	0.06	0.00
	S_{RAD}	0.06	0.16	0.10	0.00	0.01	0.01	0.00	0.02	0.01
	Q_{CM}	-0.01	-0.11	-0.26	-0.49	-0.53	-0.34	0.47	0.38	0.12
7 June	P_{SH}	0.54	0.51	0.46	0.29	0.33	0.32	0.25	0.19	0.15
	S_{HT}	-0.90	-0.92	-0.81	-0.15	-0.17	-0.23	-0.48	-0.47	-0.36
	S_{HF}	1.30	1.26	1.29	0.59	0.66	0.64	0.51	0.47	0.42
	S_{HS}	-0.03	-0.03	-0.01	0.00	0.00	0.00	-0.01	-0.01	0.00
	S_{LHLF}	0.02	0.01	0.00	0.00	0.00	0.00	0.01	0.01	0.01
	S_{RAD}	0.09	0.15	0.06	0.00	0.00	0.00	0.00	0.01	0.00
	Q_{CM}	0.05	0.03	-0.08	-0.15	-0.16	-0.09	0.20	0.17	0.09

Table 3. Thermally related surface rainfall budget (P_{SWV}, S_{HT}, S_{HF}, S_{HS}, S_{RAD}, and Q_{CM}) averaged daily and over model domain, convective regions, and raining stratiform regions in C, CNIR, and CNIM. Unit is mm h^{-1}.

Over raining stratiform regions, the elimination of microphysical effects of ice clouds decreases *PEWV* through the weakened local atmospheric moistening and reduces *PEH* through the weakened local atmospheric cooling on 4 June. During 5-6 June, the exclusion of microphysical effects of ice clouds increases *PEWV* because all rainfall processes favors rainfall in CNIM but the local atmospheric moistening reduces rainfall in CNIR. Although

the removal of microphysical effects of ice clouds barely impacts local atmospheric cooling on 5 June and it decreases local atmospheric cooling on 6 June, the decreases in stratiform rainfall are associated with the slowdown in transport of hydrometeor concentration from convective regions to raining stratiform regions. As a result, the decreases in stratiform rainfall lead to the decreases in *PEH* from CNIR to CNIM. On 7 June, the elimination of microphysical effects of ice clouds increases *PEWV* through the weakened water vapor divergence and increases *PEH* through the weakened local atmospheric cooling.

7. Conclusions

Precipitation efficiency can be well defined through diagnostic surface rainfall budgets. From thermally related surface rainfall budget, precipitation efficiency associated with heat processes (*PEH*) is first defined in this study as the ratio of surface rain rate and the rainfall source from heat and cloud budgets. Precipitation efficiency associated with water vapor processes (*PEWV*) was defined by Sui et al. (2007) as the ratio of surface rain rate to the rainfall source from water vapor and cloud budgets. In this study, both precipitation efficiencies and their responses to effects of ice clouds are investigated through an analysis of sensitivity cloud-resolving modeling data of a pre-summer heavy rainfall event over southern China during June 2008. The major results include:

- The calculations of model domain mean simulation data show that *PEH* is lower than *PEWV* because heat divergence contributes more to surface rainfall than water vapor convergence does. Precipitation efficiencies are lower during the decay phase than during the development of rainfall. *PEH* is generally lower than *PEWV* over convective regions, whereas it is generally higher than *PEWV* over raining stratiform regions. Precipitation efficiencies increase as surface rain rate increases.
- *PEWV* has different responses to radiative effects of ice clouds during the different stages of the rainfall event. The exclusion of Microphysical effects of ice clouds generally decreases *PEWV* in the calculations of model domain mean simulation data, whereas it generally increases *PEWV* over raining regions.
- The exclusion of radiative effects of ice clouds generally decreases *PEH*. The removal of microphysical effects of ice clouds generally decreases *PEH* except that it increases *PEH* over convective regions.
- Effects of ice clouds on precipitation efficiencies can be explained by the analysis of surface rainfall budgets. The changes in *PEWV* are mainly associated with the changes in local atmospheric moistening and transport of hydrometeor concentration from convective regions to raining stratiform regions during the life span of pre-summer heavy rainfall event and the change in water vapor divergence on 7 June. The changes in *PEH* are mainly related to the changes in local atmospheric cooling and radiative cooling and transport of hydrometeor concentration from convective regions to raining stratiform regions during the life span of pre-summer heavy rainfall event.

8. Acknowledgment

The authors thank W.-K. Tao at NASA/GSFC for his cloud resolving model, and Dr. N. Sun at I. M. Systems Group, Inc. for technical assistance to access NCEP/GDAS data. This study

is supported by the National Key Basic Research and Development Project of China under Grant No. 2011CB403405, the National Natural Science Foundation of China under Grant No. 41075039, the Chinese Special Scientific Research Project for Public Interest under Grant No. GYHY200806009, and the Qinglan Project of Jiangsu Province of China under Grant No. 2009.

9. References

Auer, A. H. Jr. & Marwitz, J. D. (1968) Estimates of air and moisture flux into hailstorms on the High Plains. *Journal of Applied Meteorology*, Vol.6, No.2, (April 1968), pp. 196-198, ISSN 0021-8952.

Braham, R. R. Jr. (1952) The water and energy budgets of the thunderstorm and their relation to thunderstorm development. *Journal of Meteorology*, Vol.9, No.4, (august 1952), pp. 227-242, ISSN 0095-9634.

Chong, M. & Hauser, D. (1989) A tropical squall line observed during the CORT 81 experiment in West Africa. Part II: Water budget. *Monthly Weather Rev*iew, Vol.117, No.4, (April 1989), pp. 728-744, ISSN 0027-0644.

Chou, M.-D. & Suarez, M. J. (1994) An efficient thermal infrared radiation parameterization for use in general circulation model. NASA Tech. Memo. 104606, Vol.3, pp. 1-85, Available from NASA/Goddard Space Flight Center, Code 913, Greenbelt, MD 20771.

Chou, M.-D.; Kratz, D. P. & Ridgway, W. (1991) Infrared radiation parameterization in numerical climate models. *Journal of Climate*, Vol.4, No.4, (April 1991), pp. 424-437, ISSN 0894-8755.

Chou, M.-D.; Suarez, M. J.; Ho, C.-H.; Yan, M. M.-H. & Lee K.-T., (1998) Parameterizations for cloud overlapping and shortwave single scattering properties for use in general circulation and cloud ensemble models. *Journal of Climate*, Vol.11, No.2, (February 1998), pp. 201-214, ISSN 0894-8755.

Ding, Y. (1994) Monsoon over China, Springer, ISBN 978-90-481-4161-6.

Ding Y. & Murakami, M. (1994) Asia monsoon, Meteorological Press, ISBN 7-5029-1709-8, Beijing, China.

Doswell, C. A., III; Brooks, H. E. & Maddox, R. A. (1996) Flash flood forecasting: An ingredients-based methodology. *Weather Forecasting*, Vol.11, No.4, (December 1996), pp. 560-581, ISSN 0882-8156.

Ferrier, B. S.; Simpson, J. & Tao, W.-K. (1996) Factors responsible for precipitation efficiencies in midlatitude and tropical squall simulations. *Monthly Weather Review*, Vol.124, No.10, (October 1996), pp. 2100-2125, ISSN 0027-0644.

Fovell, R. G. & Ogura, Y. (1988) Numerical simulation of a midlatitude squall line in two dimensions. *Journal of the Atmospheric Sciences*, Vol.45, No.24, (December 1988), pp. 3846-3879, ISSN 0022-4928.

Gao, S. & Li, X. (2008) Cloud-resolving modeling of convective processes. Springer, ISBN 978-1-4020-8275-7, Dordrecht.

Gao, S. & Li, X. (2010) Precipitation equations and their applications to the analysis of diurnal variation of tropical oceanic rainfall. *Journal of Geophysical Research*, Vol.115, No.D08204, (April 2010), ISSN 0148-0227.

Gao, S.; Cui, X.; Zhu, Y. & Li, X. (2005) Surface rainfall processes as simulated in a cloud resolving model. *J. Geophys. Res.*, Vol.110, No.D10202, (May 2005), ISSN 0148-0227.

Gao, S.; Ran, L. & Li, X. (2006) Impacts of ice microphysics on rainfall and thermodynamic processes in the tropical deep convective regime: A 2D cloud-resolving modeling study. *Monthly Weather Rev*iew, Vol.134, No.10, (October 2006), pp. 3015-3024, ISSN 0027-0644.

Grabowski, W. W. (2003) Impact of ice microphysics on multiscale organization of tropical convection in two-dimensional cloud-resolving simulations. *Quarterly Journal of the Royal Meteorological Society*, Vol. 129, No.587 (February 2003), pp. 67-81, ISSN 0035-9009.

Grabowski, W. W. & Moncrieff, M. M. (2001) Large-scale organization of tropical convection in two-dimensional explicit numerical simulations. *Quarterly Journal of the Royal Meteorological Society*, Vol. 127, No.572, (February 2001), pp. 445-468, ISSN 0035-9009.

Grabowski, W. W., X. Wu, and M. W. Moncrieff, 1999: Cloud-resolving model of tropical cloud systems during Phase III of GATE. Part III: Effects of cloud microphysics. *Journal of the Atmospheric Sciences*, Vol.56, No.14, (July 1999), pp. 2384-2402, ISSN 0022-4928.

Heymsfield, G. M. & Schotz, S. (1985) Structure and evolution of a severe squall line over Oklahoma. *Monthly Weather Review*, Vol.113, No.9, (September 1985), pp. 1563-1589, ISSN 0027-0644.

Houghton, H. G. (1968) On precipitation mechanisms and their artificial modification. *Journal of Applied Meteorology*, Vol.7, No.5, (October 1968), pp. 851-859, ISSN 0021-8952.

Hsie, E. Y.; Farley, R. D. & Orville, H. D. (1980) Numerical simulation of ice phase convective cloud seeding. *Journal of Applied Meteorology*, Vol.29, No.8, (August 1980), pp. 950-977, ISSN 0021-8952.

Krishnamurti, T. N.; Molinari, J. & Pan, H.-L. (1976) Numerical simulation of the Somali Jet, *Journal of the Atmospheric Sciences*, Vol.33, No.12, (December 1976), pp. 2350-2362, ISSN 0022-4928.

Krueger, S. K.; Fu, Q.; Liou, K.-N. & Chin, H.-N. S. (1995) Improvement of an ice-phase microphysics parameterization for use in numerical simulations of tropical convection, *Journal of Applied Meteorology*, Vol.34, No.1, (Janrary 1995), pp. 281-287, ISSN 0021-8952.

Li, X.; Sui, C.-H.; Lau, K.-M. & Chou, M.-D. (1999) Large-scale forcing and cloud-radiation interaction in the tropical deep convective regime. *Journal of the Atmospheric Sciences*, Vol.56, No.17, (September 1999), pp. 3028-3042, ISSN 0022-4928.

Li, X.; Sui, C.-H. & Lau, K.-M. (2002) Precipitation efficiency in the tropical deep convective regime: A 2-D cloud resolving modeling study. *Journal of Meteorological Society of Japan*, Vol.80, No.2, (April 2002), pp. 205-212, ISSn 0026-1165.

Lin, Y.-L.; Farley, R. D. & Orville, H. D. (1983) Bulk parameterization of the snow field in a cloud model, *Journal of Applied Meteorology and climatology*, Vol.22, No.6, (June 1983), pp. 1065-1092, ISSN 0733-3021.

Liu, C.; Moncrieff, M. W. & Zipser, E. J. (1997): Dynamic influence of microphysics in tropical squall lines: A numerical study. *Monthly Weather Review*, Vol.125, No.9, (September 1997), pp. 2193-2210, ISSN 0027-0644.

McCumber, M.; Tao, W.-K.; Simpson, J.; Penc, R. & Soong, S.-T. (1991) Comparison of ice – phase microphysical parameterization schemes using numerical simulations of

tropical convection. *Journal of Applied Meteorology and Climatology*, Vol.30, No.7, (July 1991), pp. 985-1004, ISSN 0894-8763.

Nicholls, M. E. (1987) A comparison of the results of a two-dimensional numerical simulation of a tropical squall line with observations. *Monthly Weather Review*, Vol.115, No.12, (December 1987), pp. 3055-3077, ISSN 0027-0644.

Ping, F.; Luo, Z. & Li, X. (2007) Microphysical and radiative effects of ice microphysics on tropical equilibrium states: A two-dimensional cloud-resolving modeling study. *Monthly Weather Review*, Vol.135, No.7, (July 2007), pp. 2794-2802, ISSN 0027-0644.

Rutledge, S. A. & Hobbs, P. V. (1983) The mesoscale and microscale structure and organization of clouds and precipitation in midlatitude cyclones. Part VIII: A model for the "seeder-feeder" process in warm-frontal rainbands, *Journal of the Atmospheric Sciences*, Vol.40, No.5, (May 1983), pp. 1185-1206, ISSN 0022-4928.

Rutledge, S. A. & Hobbs, P. V. (1984) The mesoscale and microscale structure and organization of clouds and precipitation in midlatitude cyclones. Part XII: A diagnostic modeling study of precipitation development in narrow cold-frontal rainbands, *Journal of the Atmospheric Sciences*, Vol.41, No.20., (October 1984), 2949-2972, ISSN 0022-4928.

Shen, X.; Wang, Y.; Zhang, N. & Li, X. (2010) Precipitation and cloud statistics in the deep tropical convective regime. *Journal of Geophysical Research*, Vol.115, No.D24205, ISSN 0747-7309.

Shen, X.; Wang, Y. & Li, X. (2011) Radiative effects of water clouds on rainfall responses to the large-scale forcing during pre-summer heavy rainfall over southern China. *Atmospheric Research*, Vol.99, No.1, (January 2011), pp.120-128, ISSN0169-8095.

Shen, X.; Wang, Y. & Li, X. (2011) Effects of vertical wind shear and cloud radiatve processes on responses of rainfall to the large-scale forcing during pre-summer heavy rainfall over southern China. *Quarterly Journal of the Royal Meteorological Society*, Vol.137, No.654, (February 2011), pp. 236-249, ISSN 0035-9009.

Simmonds, I.; Bi, D. & Hope, P. (1999) Atmospheric water vapor flux and its association with rainfall over China in summer. *Journal of Climate*, Vol.12, No.5, (May 1999), pp. 1353-1367, ISSN 0894-8755.

Soong, S. T. & Ogura, Y. (1980) Response of tradewind cumuli to large-scale processes. *Journal of the Atmospheric Sciences*, Vol.37, No.9, (Spetember 1980), pp. 2035-2050, ISSN 0022-4928.

Soong, S. T., and W. K. Tao, 1980: Response of deep tropical cumulus clouds to mesoscale processes. *Journal of the Atmospheric Sciences*, Vol.37, No.9, (Spetember 1980), pp. 2016-2034, ISSN 0022-4928.

Sui, C.-H. & Li, X. (2005) A tendency of cloud ratio associated with the development of tropical water and ice clouds. *Terrestrial Atmospheric and Oceanic Sci*ences, Vol.16, No.4, (June 2005), pp. 419-434, ISSN 1017-0839.

Sui, C.-H.; Lau, K.-M.; Tao, W.-K. & Simpson, J. (1994) The tropical water and energy cycles in a cumulus ensemble model. Part I: Equilibrium climate. *Journal of the Atmospheric Sciences*, Vol. 51, No.5, (March 1994), pp. 711-728, ISSN 0022-4928.

Sui, C.-H.; Li, X. & Lau, K.-M. (1998) Radiative-convective processes in simulated diurnal variations of tropical oceanic convection, *Journal of the Atmospheric Sciences*, Vol.55, No.13, (July 1998), pp. 2345-2359, ISSN 0022-4928.

Sui, C.-H.; Li, X.; Yang, M.-J. & Huang, H.-L. (2005) Estimation of oceanic precipitation efficiency in cloud models. *Journal of the Atmospheric Sciences*, Vol.62, No.12, (December 2005), pp. 4358-4370, ISSN 0022-4928.

Sui, C.-H.; Li, X. & Yang, M.-J. (2007) On the definition of precipitation efficiency. *Journal of the Atmospheric Sciences*, Vol. 64, No.12, (December 2007), pp 4506-4513, ISSN 0022-4928.

Tao, S. & Ding, Y. (1981) Observational evidence of the influence of the Qinghai-Xizang (Tibet) plateau on the occurrence of heavy rain and severe convective storms in China. *Bulletin of American Meteorological Society*, Vol.62, No.1, (January 1981), pp. 23-30, ISSN 0003-0007.

Tao, W.-K. & Simpson, J. (1989) Modeling study of a tropical squall-type convective line, *Journal of the Atmospheric Sciences*, Vol.46, No.1, (January 1989), pp. 177-202, ISSN 0022-4928.

Tao, W.-K. & Simpson, J. (1993) The Goddard Cumulus Ensemble model. Part I: Model description. *Terrestrial Atmospheric and Oceanic Sci*ences, Vol.4, No. 1, (March 1993), pp. 35-72, ISSN 1017-0839.

Tao, W.-K; Simpson J. & McCumber, M. (1989) An ice-water saturation adjustment, *Monthly Weather Review*, Vol.117, No.1, (January 1989), pp. 231-235, ISSN 0027-0644.

Tao, W.-K.; Simpson, J. & Soong, S.-T. (1991) Numerical simulation of a subtropical squall line over the Taiwan Strait. *Monthly Weather Review*, Vol.119, No.11, (November 1991), pp. 2699-2723, ISSN 0027-0644.

Tao, W.-K.: Simpson, J.; Sui, C.-H.; Ferrier, B.; Lang, S.; Scala, J.; Chou M.-D. & Pickering, K. (1993) Heating, moisture and water budgets of tropical and midlatitude squall lines: Comparisons and sensitivity to longwave radiation. *Journal of the Atmospheric Sciences*, Vol.50, No.5, (March 1993), pp. 673-690, ISSN 0022-4928.

Wang, D.; Li, X.; Tao, W.-K.; Liu, Y. & Zhou, H. (2009) Torrential rainfall processes associated with a landfall of severe tropical strom Bilis (2006): A two-dimensional cloud-resolving modeling study. *Atmospheric Res*earch, Vol.91, No.1, (January 2009), pp. 94-104 ISSN 0169-8095.

Wang, J. & Li, M. (1982) Cross equator flow from Australia and summer monsoon circulations and precipitation over China. *Sci. Atmos. Sin*, Vol.6, No.1, (January 1982), pp. 1-10, ISSN 1006-9895.

Wang, Y.; Shen, X. & Li, X. (2010) Microphysical and radiative effects of ice clouds on responses of rainfall to the large-scale forcing during pre-summer heavy rainfall over southern China. *Atmospheric Research*, Vol.97, No.1-2, (July 2010), pp. 35-46, ISSN 0169-8095.

Wu, X. (2002) Effects of ice microphysics on tropical radiative-convective-oceanic quasi-equilibrium states. *Journal of the Atmospheric Sciences*, Vol.59, No.11, (June 2002), 1885-1897, ISSN 0022-4928.

Wu, X.; Hall, W. D.; Grabowski, W. W.; Moncrieff, M. W.; Collins, W. D. & Kiehl, J. T. (1999) Long-term behavior of cloud systems in TOGA COARE and their interactions with radiative and surface processes. Part II: Effects of ice microphysics on cloud-radiation interaction. *Journal of the Atmospheric Sciences*, Vol.56, No.18, (September 1999), pp. 3177-3195, ISSN 0022-4928.

Xu, X.; Xu, F. & Li, B. (2007) A cloud-resolving modeling study of a torrential rainfall event over China. *Journal of Geophysical Research*, Vol.112, No.D17204, ISSN 0148-0227.

Yoshizaki, M. (1986) Numerical simulations of tropical squall-line clusters: Two-dimensional model. *Journal of Meteorological Society of Japan*, Vol.64, No.4, (August 1986), pp. 469-491, ISSN 0026-1165.

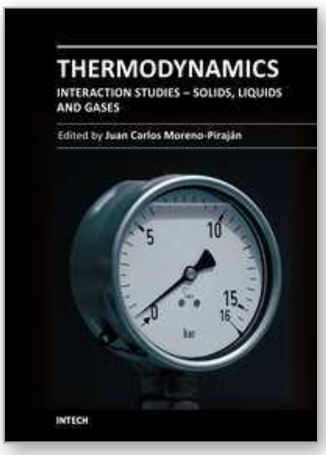

Thermodynamics - Interaction Studies - Solids, Liquids and Gases
Edited by Dr. Juan Carlos Moreno PirajÃ¡n

ISBN 978-953-307-563-1
Hard cover, 918 pages
Publisher InTech
Published online 02, November, 2011
Published in print edition November, 2011

Thermodynamics is one of the most exciting branches of physical chemistry which has greatly contributed to the modern science. Being concentrated on a wide range of applications of thermodynamics, this book gathers a series of contributions by the finest scientists in the world, gathered in an orderly manner. It can be used in post-graduate courses for students and as a reference book, as it is written in a language pleasing to the reader. It can also serve as a reference material for researchers to whom the thermodynamics is one of the area of interest.

How to reference
In order to correctly reference this scholarly work, feel free to copy and paste the following:

Xinyong Shen and Xiaofan Li (2011). Thermodynamic Aspects of Precipitation Efficiency, Thermodynamics - Interaction Studies - Solids, Liquids and Gases, Dr. Juan Carlos Moreno PirajÃ¡n (Ed.), ISBN: 978-953-307-563-1, InTech, Available from: http://www.intechopen.com/books/thermodynamics-interaction-studies-solids-liquids-and-gases/thermodynamic-aspects-of-precipitation-efficiency

INTECH
open science | open minds

InTech Europe
University Campus STeP Ri
Slavka Krautzeka 83/A
51000 Rijeka, Croatia
Phone: +385 (51) 770 447
Fax: +385 (51) 686 166
www.intechopen.com

InTech China
Unit 405, Office Block, Hotel Equatorial Shanghai
No.65, Yan An Road (West), Shanghai, 200040, China
中国上海市延安西路65号上海国际贵都大饭店办公楼405单元
Phone: +86-21-62489820
Fax: +86-21-62489821